Cancer Cell International

RESEARCH Open Access

Stearoyl CoA desaturase inhibition can effectively induce apoptosis in bladder cancer stem cells

Yuchen Li[1], Chiyuan Piao[1*] and Chuize Kong[1*]

Abstract
Bladder cancer stands as one of the most prevalent cancers worldwide. While our previous research confirmed the significant role of stearoyl-CoA desaturase (SCD) in bladder cancer, the underlying reasons for its abnormal overexpression remain largely unknown. Moreover, the distinct response to SCD inhibitors between cancer stem cells (CSCs) and adherent cultured cell lines lacks clear elucidation. Therefore, in this experiment, we aim to conduct an analysis and screening of the SCD transcription start site, further seeking critical transcription factors involved. Simultaneously, through experimental validation, we aim to explore the pivotal role of endoplasmic reticulum stress/unfolded protein response in drug sensitivity among cancer stem cells. Additionally, our RNA-seq and lipid metabolism analysis revealed the significant impact of nervonic acid on altering the proliferative capacity of bladder cancer cell lines.

Keywords Bladder cancer, Stearoyl-CoA desaturase, DNA damage (DDR), Cancer stem cells (CSCs), Apoptosis, ER stress, Nervonic acid

Introduction

Cancer has consistently been a significant factor affecting public health worldwide. Despite long-term and relentless efforts, the number of deaths caused by cancer is decreasing year by year. However, malignant tumors remain the second leading cause of human mortality globally. Among them, bladder cancer ranks as the fourth most common malignancy in men [1, 2]. According to the report from the National Central Cancer Registry of China (NCCR) in 2016, the incidence rate of bladder cancer ranks sixth among malignant tumors in males [3].

Currently, there are continuous improvements in the medical diagnostic methods and surgical approaches for bladder tumors. To enhance the treatment of bladder cancer, ongoing research is focused on developing more accurate diagnostic methods and classifying bladder cancer based on molecular genetic levels [4–6]. However, despite advancements in existing diagnostic and treatment technologies, there has been limited improvement in the recurrence and progression of bladder tumors. The insufficient understanding of the pathological and physiological characteristics, as well as the biological mechanisms underlying the recurrence and progression of this disease, remains a significant challenge [7, 8].

Therefore, a comprehensive investigation into the biological mechanisms of the occurrence, recurrence, and progression of bladder tumors holds paramount

*Correspondence:
Chiyuan Piao
cypiao@cmu.edu.cn
Chuize Kong
kongchuize_cmu@sina.cn
[1]Department of Urology, The First Hospital of China Medical University, No. 155 Nanjing North Street, Heping District, Shenyang City 110000, Liaoning Province, People's Republic of China

importance for the diagnosis, treatment, and improvement of prognosis for this disease.

Stearoyl-CoA desaturase (SCD), a transmembrane protein located in the endoplasmic reticulum, plays a crucial role in lipid metabolism. Initially associated with metabolic syndromes such as obesity, fatty liver, dyslipidemia, and insulin resistance, SCD has been implicated in various processes related to cancer. With the development of lipid omics and genomics, the significance of SCD and its product monounsaturated fatty acids (MUFA) in tumors has gradually become understood. The ratio of monounsaturated fatty acids to saturated fatty acids (SFA) in the serum and tissues of cancer patients can be used to assess cancer risk, and the conversion between SFA and MUFA is closely associated with tumor prognosis [9].

Oleic acid (OA) is a crucial substrate for SCD. When SCD expression is upregulated, stearic acid can be converted to OA under the action of SCD. Conversely, when SCD is downregulated, OA gradually converts to stearic acid. In recent years, as lipid metabolism in tumors is under investigation, attention has increasingly turned to OA, a common monounsaturated fatty acid in the human body. Several studies indicate that OA can promote proliferation and invasion in breast cancer, cervical cancer, colon cancer, and other tumors by activating pathways such as Erk, Akt, MAPK, etc [10–12].

The sustained activation of SCD in cancer cells provides a continuous supply of MUFA substrates, promoting lipid biosynthesis, and participates in the signaling pathways for cancer cell proliferation and survival, accelerating cell growth, increasing invasion, and enhancing survival capabilities. Early research found that the secretion and transport of Wnt3a protein depend on the palmitoylation of specific sites [13]. Wnt signal activation leads to decreased phosphorylation of GSK3β, causing β-catenin to accumulate in the nucleus and promoting tumor occurrence and metastasis. Blocking the synthesis of monounsaturated fatty acids using SCD inhibitors such as CAY-10,566 and A939572 inhibits the paracrine and autocrine secretion of Wnt proteins, thereby suppressing downstream Wnt signaling activation [14]. Unsaturated fatty acids can also directly inhibit the degradation of β-catenin, promoting tumor growth. Fas-associated factor 1 (FAF1) binds to β-catenin and promotes its degradation. Unsaturated fatty acids, by binding to the UAS domain of this protein, hinder the ubiquitination and degradation of β-catenin [15]. Moreover, recent research has discovered that SCD in tumors can support continuous proliferation of cancer cells through bypass pathways, ensuring their growth and survival even when other pathways are inhibited to varying degrees [16].

We have elaborated for the first time on the relationship between SCD gene activity and bladder cancer [17]. Importantly, we induced bladder cancer stem cells (CSCs) from human bladder cancer cell lines through suspension culture and conducted a microarray assay to further identify DEGs. By integrating clinical data, we ultimately identified SCD as the most crucial target. Subsequent in vitro experiments demonstrated that SCD significantly promotes the proliferation and invasion of cancer cells. Finally, we tested whether SCD inhibitors could enhance chemotherapy sensitivity, but we did not obtain positive results. Thus, we conclude that high levels of SCD expression in patients with urothelial bladder cancer indicate a poor prognosis. Furthermore, inhibiting SCD gene activity significantly suppresses the proliferation and invasion of bladder cancer cells. Unlike many other cancer types, inhibiting SCD may not improve the efficacy of conventional chemotherapy for bladder cancer. However, SCD inhibitors may specifically target CSCs, inhibiting their proliferation and inducing apoptosis in CSCs of patients with bladder cancer. To explore the reasons behind the abnormally high expression of SCD and the unique drug response in CSCs, we attempted mechanistic analysis through this study.

Materials and methods

Cell culture

Bladder cancer cell lines T24 and UMUC3 were propagated in RPMI-1640 medium, whereas RT4 cells utilized McCoy's 5 A medium. Both types of media contained 10% fetal bovine serum. All cell lines were sourced from the Type Culture Collection at the Chinese Academy of Sciences in Shanghai and kept under conditions of 37 °C and 5% CO_2 in a humidified environment. When cell cultures exceeded 80% confluence, they were rinsed with 1× PBS and subsequently subjected to trypsinization at 37 °C for passaging.

Isolation and propagation of BCSCs

Bladder cancer cell line UMUC3 were first dissociated using a 0.25% trypsin/EDTA solution, then plated into ultralow attachment flasks (Corning) at a concentration of 10,000 cells per milliliter. The cells were cultured in a serum-free medium composed of a 1:1 ratio of DMEM and F12, enhanced with B27 supplement (Invitrogen), along with 20 ng/mL of recombinant epidermal growth factor (EGF) and 10 ng/mL of recombinant basic fibroblast growth factor (bFGF), both supplied by Invitrogen. Cancer stem cells (CSCs) were cultured for a period of 7 to 10 days for each generation. Sphere cells were then harvested, passaged using trypsin, and re-suspended in the same serum-free medium. Cells from the third-generation spheres were selected for further experimental use.

CCK-8-3D assay for detecting the proliferation activity of cancer stem cells

Add 100 μl of cell suspension containing 5000 cells per well. Simultaneously, set up wells with cell-free culture medium as negative controls and follow the 3D cell culture protocol. Perform drug treatment according to the specific experimental design. Subsequently, add 10 μl of CCK-3D solution per well. Include wells with cell culture medium, drug, and CCK-3D solution without cells as blank controls if concerned about potential interference from the drug. Then, incubate the 96-well plate in the cell culture incubator for 2 h. After incubation, gently tap the plate to mix the orange-yellow formazan in each well and measure the absorbance at 450 nm wavelength.

Gene expression analysis by quantitative RT-PCR

RNA was isolated from both whole bladder cancer tissues and cultured bladder cancer cells using TRIzol reagent, followed by DNase I treatment to eliminate any contaminating DNA. The purified RNA was then used to synthesize cDNA with the PrimeScript RT Master Mix. For quantitative RT-PCR, SYBR Premix Ex Taq was employed on a LightCycler system. The expression levels were normalized against glyceraldehyde-3-phosphate dehydrogenase (GAPDH), which served as the internal control gene.

Western blot

Whole-protein lysates were obtained using a radioimmunoprecipitation assay (RIPA) buffer, which included protease and phosphatase inhibitors to prevent protein degradation. Proteins were separated via 10% SDS-PAGE, applying a voltage of 140 V. Subsequently, the proteins were transferred onto 0.2 μm PVDF membranes using a Bio-Rad mini-transblot apparatus at a current of 350 mA. The membranes were blocked for 2 h at room temperature with 5% non-fat milk to prevent non-specific binding. This was followed by an overnight incubation at 4 °C with primary antibodies, and then a 45-minute incubation with corresponding secondary antibodies. Detection of the proteins was performed using the Luminata substrate, and quantitative analysis of the immunoblot bands was carried out using ImageJ software.

Chromatin immunoprecipitation (ChIP)

Perform the ChIP assay using the SimpleChIP® Enzymatic Chromatin IP kit (9002S, Cell Signaling Technology) following the manufacturer's instructions. For optimal ChIP results, a minimum of 10^7 cells is required to include positive and negative controls. Cells were cross-linked with 1% formaldehyde for 10 minutes, and the reaction was halted by adding glycine. Scraped cells were suspended in cold buffer (ice-cold PBS+protease inhibitor cocktail) for immediate nuclei preparation and chromatin digestion using micrococcal nuclease. Subsequently, cancer cell nuclei were fully lysed after three sets of 20-second pulses using a sonicator at setting 6 with a 1/8-inch probe. DNA fragments should be digested to approximately 150–900 bp. Chromatin was immunoprecipitated using negative control IgG (2729, Cell Signaling Technology, 1 μl) or positive control Histone H3 (4620, Cell Signaling Technology, 10 μl) or TFAP2A (sc-12726 X, Santa Cruz, 10 μl) primary antibodies. Following elution of chromatin from antibody/protein G agarose beads and reversal of cross-linking, the eluted DNAs were quantified using rt-qPCR. The primer sequences are listed below: ChIP-qPCR primers for RPL30 as a positive control were purchased from Cell Signaling Technology (7014, Cell Signaling Technology). SCD primer 1, forward 5′-CAAAACATCCCGCACGCATC −3′, reverse 5′-GCT GGTGTGTGTGTGCCT-3′; SCD primer 2, forward 5′-G CTGGTGTGTGTGTGCCT-3′, reverse 5′-GTACGCCT GCGAACAATGG-3′; SCD primer 3, forward 5′-AAGC TCCAGATCCTGGGGTG-3′, reverse 5′-AAACAGTGG TGAACCCTCGG-3′; SCD primer 4, forward 5′-CCGA GGGTTCACCACTGTTT-3′, reverse 5′-TCGGGAGCT TTCTCTCTGGA-3′; SCD primer 5, forward 5′-CTGAG AAGGAGAAACAGAGGGG-3′, reverse 5′-CTGTAAA CTCCGGCTCGTCAT-3′; SCD primer 6, forward 5′-TC ATTAGCATTTCCCCAGAGGC-3′, reverse 5′-GGTCC CGCGTGGAGGTAAG-3′; SCD primer 7, forward 5′-C TTACCTCCACGCGGGACC-3′, reverse 5′-CCCGAGC CGGGAATTTAAAGG-3′; SCD primer 8, forward 5′-G CCTTTAAATTCCCGGCTCG-3′, reverse 5′-CCGGAG GACTGCGGTTTC-3′; SCD primer 9, forward 5′-GCT TCGAAACCGCAGTCCTC-3′, reverse 5′-GGCTGGGA AACTCACATCGT-3′; SCD primer 10, forward 5′-TTG CTGCAGGACGATGTGAG-3′, reverse 5′-GGAAGGC AGCACAACTCGAA-3′; SCD primer 11, forward 5′-GC CTTCCGTGAGTTGGGAAT-3′, reverse 5′-CTCACAT CCCCACGAAGACAA-3′; SCD primer 12, forward 5′-C TTCGTGGGGATGTGAGTGC-3′, reverse 5′-GGTAGG GTGTATCCGAGACG-3′; SCD primer 13, forward 5′-T ACCCTCAGTGAACTACGGC-3′, reverse 5′-AGATCT GGAAGGGGGAGGAA-3'; SCD primer 14, forward 5′-ACGATGCCCCTCTACTTGGA-3′, reverse 5′- GGCTC CCAAGTGTAGCAGAG-3′; SCD primer 15, forward 5′-TCTGGAGAAACATCATCCTTATGTC-3′, reverse 5′-GAGCAGTGAGTACCTGGAGGA-3′; SCD primer 16, forward 5′- GTAAGCAGCCTCCCTGTCCT-3′, reverse 5′- CACTAGGCCTGAAGCAACCAA-3'.

Dual luciferase reporter assay

293T cells were seeded and cultured in 24-well plates. Subsequently, co-transfection was performed using Lipofectamine 3000 reagent with 1 μg of promoter reporter vectors and 10 ng of Renilla luciferase expression vector (pRL-CMV), along with either the empty vector or

TFAP2A-wildtype or TFAP2A-mutant type expression vector. After 48 h post-transfection, cells were lysed, and the promoter activities were measured using the Dual-Luciferase Reporter Assay System Kit (E1910; Promega).

5-ethynyl-2′-deoxyuridine assay

Flow cytometry analysis was performed using a FACS-Calibur Flow Cytometer with a 488 nm excitation laser. UMUC3 cells, following specific pre-treatments, were exposed to 50 μmol/L of 5-ethynyl-2′-deoxyuridine (EdU) (provided by the Cell-Light™ EdU Apollo®488 In Vitro Flow Cytometry Kit, Guangzhou RiboBio, China) for 24 h, followed by an additional 4-hour incubation. The staining process was initiated by removing the EdU medium and fixing the cells with 4% paraformaldehyde for 15 min at room temperature. Cells were then washed with a 2 mg/mL glycine solution for 5 min, permeabilized using 0.5% Triton X-100 for 10 min, and washed twice with PBS. To facilitate the click reaction, a mixture containing Tris-HCl (pH 8.5, 100 mmol/L), CuSO4 (1 mmol/L), Apollo 488 azide (100 μmol/L), and ascorbic acid (100 mmol/L) was added for 10 min under light-protected conditions. After two additional washes with 0.5% Triton X-100, cells were resuspended in 150 μL PBS. Data acquisition and analysis were conducted using BD CellQuest Pro software.

Real-time cell analysis (RTCA) for cell proliferation

To initiate the experiment, 50 μl of culture medium is added to the device, left at room temperature for 1 min, and placed on the testing platform to establish a baseline. For optimal experimental conditions, maintain cell density between 70% and 80% in the laboratory and preferably within the logarithmic growth phase. When conducting the experiment, retrieve the cells from the incubator, wash once with PBS, digest with 0.25% trypsin solution, terminate digestion with culture medium, centrifuge the cells with medium, remove the supernatant, resuspend the cells in fresh medium, and perform cell counting under an inverted microscope. Calculate cell density using the formula: Cell number/ml of original suspension = (total cell count in 4 large squares / 4) * 10,000 * dilution factor. Prepare cell suspensions at the desired concentrations. Seed the appropriately prepared cell suspension into the pre-baselined device at 100ul per well, let it sit at room temperature for 30 min, then place it into the CO2 incubator on the testing platform to commence detection. Subsequently, propagate the remaining cells at an appropriate density for further passages in culture flasks within the CO2 incubator for future use. Finally, administer the drug treatment the following day and observe the results after 72 h.

Metabolites extraction

Samples were extracted using 1000 μL of a solvent mixture composed of isopropanol and hexane in a 2:3 ratio. An internal standard, 5 μL of Trans C17 at a concentration of 2 mg/L, was added, followed by vortex mixing for 5 min. The mixture was homogenized using a ball mill for 30 s, repeated three times, and then subjected to ultrasound treatment for 5 min while being kept in ice water. Afterward, samples were centrifuged at 12,000 rpm for 2 min at 4 °C, and 400 μL of the supernatant was collected. The collected supernatant was completely dried using a vacuum concentrator without heating. Subsequently, 200 μL of methanol was added to dissolve the residue for derivatization, followed by drying under a nitrogen stream. To the dried sample, 80 μL of methanol was added to re-dissolve it. Finally, all prepared samples were analyzed using gas chromatography-mass spectrometry (GC-MS).

Library construction and sequencing

Following the extraction of total RNA, eukaryotic mRNA was isolated using Oligo(dT) beads, while prokaryotic mRNA enrichment involved the depletion of rRNA using the Ribo-Zero™ Magnetic Kit (Epicentre). The isolated mRNA was then fragmented into smaller pieces using a fragmentation buffer. These fragments were converted into cDNA through reverse transcription utilizing random primers. The synthesis of the second cDNA strand involved DNA polymerase I, RNase H, dNTPs, and an appropriate reaction buffer. The resulting cDNA was purified using the QiaQuick PCR extraction kit, subjected to end repair, polyadenylation, and ligated to Illumina sequencing adapters. Subsequently, the ligated products were size selected via agarose gel electrophoresis, amplified by PCR, and sequenced using the Illumina HiSeq™ 2500 platform, provided by Gene Denovo Biotechnology Co. (Guangzhou, China).

Differentially expressed genes (DEGs) analysis

The edgeR package (http://www.rproject.org/) was employed to identify differentially expressed genes (DEGs) across various sample groups. Genes exhibiting a fold change of 2 or greater and a false discovery rate (FDR) below 0.05 were classified as significant DEGs. These identified DEGs were subsequently analyzed for enrichment in Gene Ontology (GO) functions and Kyoto Encyclopedia of Genes and Genomes (KEGG) pathways to determine their biological significance.

GO enrichment analysis and pathway enrichment analysis

The Gene Ontology (GO) framework is a globally recognized system for classifying gene functions, utilizing a continually updated controlled vocabulary to provide detailed descriptions of gene properties and

their associated products across different organisms. GO categorizes these functions into three main ontologies: molecular function, cellular component, and biological process. Each specific function within GO is represented as a GO term, which is categorized under one of these ontologies. GO enrichment analysis identifies GO terms that are significantly overrepresented among differentially expressed genes (DEGs) when compared to a genomic background, thereby highlighting DEGs involved in specific biological roles. Initially, DEGs are mapped to GO terms using the Gene Ontology database (http://www.geneontology.org/), and the frequency of each term is calculated. GO terms showing significant enrichment among DEGs relative to the genome background are identified using a hypergeometric test.

Genes often interact in complex networks to carry out specific biological functions, which can be better understood through pathway-based analyses. The Kyoto Encyclopedia of Genes and Genomes (KEGG) serves as a primary resource for pathway information [6]. Pathway enrichment analysis is used to pinpoint pathways, such as metabolic or signal transduction pathways, that are significantly overrepresented in DEGs compared to the overall genome, providing deeper insights into gene function and interaction.

Apoptosis detection by flow cytometry

To evaluate apoptosis, the FITC Annexin V Apoptosis Detection Kit from BD Pharmingen was utilized. After the treatment, cells were trypsinized gently and rinsed with a medium containing serum. The cells were then harvested via centrifugation, washed with PBS, and resuspended in 1X Binding Buffer. They were subsequently stained with annexin V-FITC and propidium iodide (PI) for 5 min at room temperature, protected from light, as per the manufacturer's guidelines. Finally, the stained cells were analyzed using the FACS Calibur Flow Cytometer.

Subcutaneous xenograft mouse model and dosing regimen

The UMUC3 cells were subcutaneously injected into the back of Balb/c nude mice (6-week-old, female, 20 gram) at a cell count of $5*10^6$. Observations were made every 3–5 days. When the tumor size reached approximately $50mm^3$, the mice were randomly assigned to different treatment groups within each genotype. Three treatment groups were established: a vehicle-treated group ($n=5$) as control group, an A939572-treated group ($n=5$) and an A939572-treated + nervonic acid-treated ($n=5$). The vehicle used consisted of a solution containing 10% DMSO, 40% PEG300, 5% Tween-80, and 45% Saline. A939572 (MedChem Express, HY-50709) and nervonic acid (MedChem Express, HY-N2526) were administered orally at a dose of 30 mg/kg twice daily for 3 weeks. The mice were euthanized, and tumor weights were measured to compare tumor sizes. Balb/c nude mice were purchased from Vital River. The immune status of Balb/c nude mice is characterized by the lack of effective T-cell development due to thymic abnormalities. They are genetically modified as mutants (hairless mutation) with a genotype of Foxn1 < nu>.

The animal experiments adhered to the guidelines outlined in the 8th edition of the Guide for the Care and Use of Laboratory Animals by the US National Institutes of Health (published by the National Academies Press in 2011). Approval for all procedures was obtained from the Ethics Committee for Animal Experimentation of China Medical University. All animals were treated with care and respect, and every effort was made to minimize both the number of animals used and any associated suffering. We maintained the animals' housing environment as stable and consistent as possible throughout the experiment. This included controlling factors such as room temperature, humidity, and lighting to ensure that the animals lived in similar environmental conditions. During the experiment, if the size of the subcutaneous tumor exceeds 2 cm or if signs of distress appear, the experiment will be immediately terminated.

Statistical analysis

Results are expressed as either individual data points or as mean ± standard deviation (SD) unless noted otherwise. Statistical analyses were performed using GraphPad Prism 9 (GraphPad Software). For comparisons between two groups, statistical significance was evaluated using a two-tailed Student's t-test for normally distributed data and the Mann-Whitney U test for non-normally distributed data. In the case of multiple group comparisons, one-way ANOVA followed by Dunnett's post hoc test was applied to data with a normal distribution. For data not following a normal distribution, the Kruskal-Wallis test was used, followed by Dunn's post hoc test to assess differences between groups and controls. Correlations were assessed using Spearman's rank correlation coefficient, a nonparametric method.

Results

TFAP2A plays a significant role in the transcriptional regulation of SCD in bladder cancer

In previous studies, we observed highly active transcriptional activity of SCD in induced bladder cancer stem cells. To explore the reasons for SCD transcriptional activation, we conducted various experiments. First, we examined the methylation levels of the SCD gene promoter region in bladder cancer and normal bladder mucosal tissues using the UALCAN database. The results showed that the SCD promoter region in both bladder

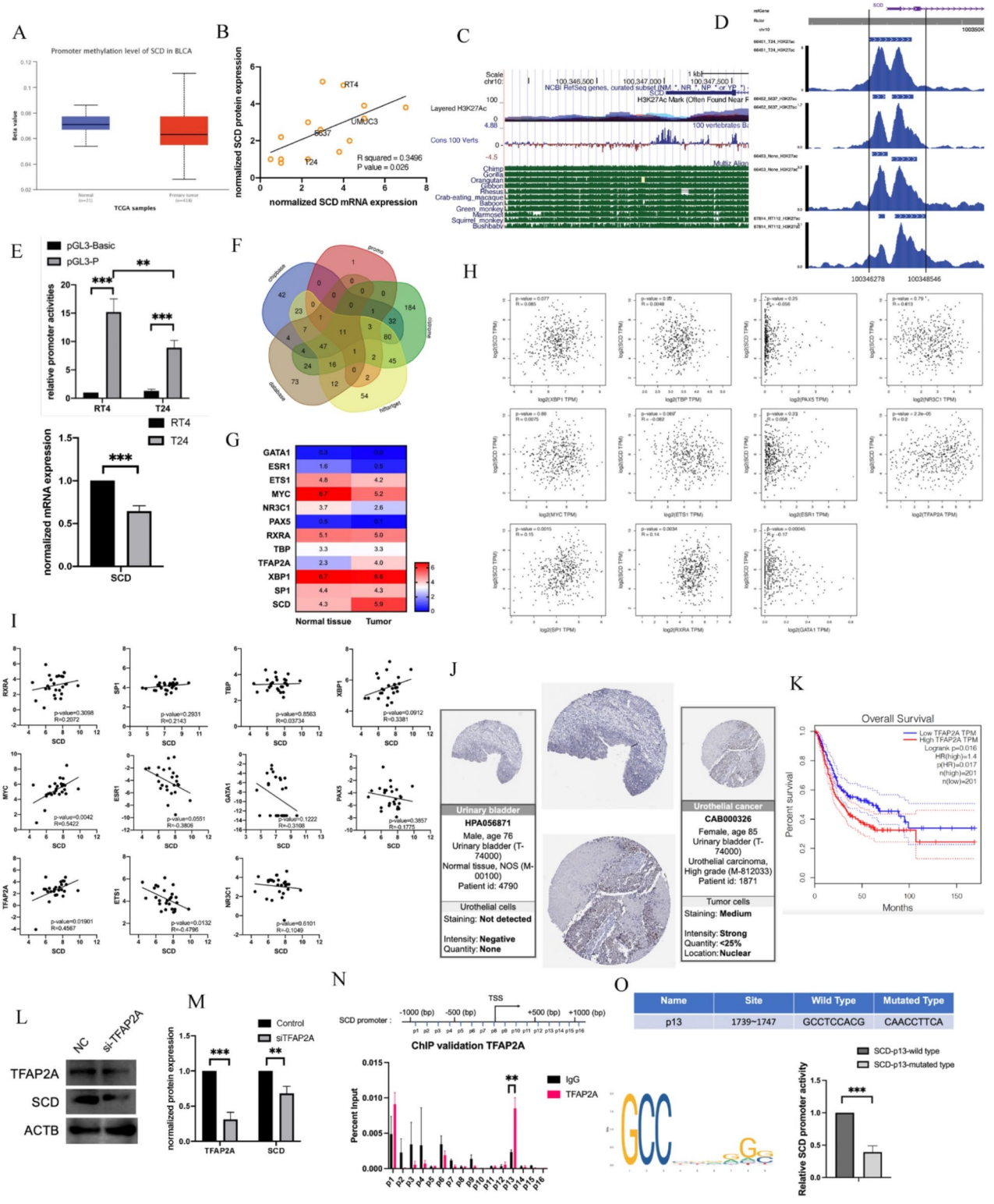

Fig. 1 (See legend on next page.)

(See figure on previous page.)

Fig. 1 TFAP2A significantly contributes to the transcriptional control of SCD in bladder scancer. (**A**) Assessment of the methylation level of the SCD promoter region. (https://ualcan.path.uab.edu/); (**B**) the mRNA and protein expression of SCD in 10 bladder cancer tissue specimens and common bladder cancer cell lines (*p* value = 0.026); (**C**) and (**D**) the conservation of the SCD promoter and the core promoter region of SCD in bladder cancer cell lines; (**E**) Construct luciferase reporter gene plasmids based on the core promoter region and verify its transcriptional activity through transfection; (**F**) Predictive analysis of the core promoter region for binding transcription factors through multiple database integration; (**G**) The expression profiles of the 11 transcription factors selected through analysis using TCGA database; (**H**) and (**I**) The correlation analysis between the expression levels of SCD and the alternative 11 transcription factors (TCGA and CCLE databases); (**J**) Check the immunohistochemistry of TFAP2A in the bladder mucosa and bladder cancer on the Human Protein Atlas; (**K**) The impact of high and low expression levels of TFAP2A (median) on the survival of bladder cancer patients analyzed using TCGA database (Log rank $p = 0.016$); (**L**) and (**M**) After knocking down TFAP2A, the protein expression levels of both TFAP2A and SCD; (**N**) and (**O**) Validation of the direct binding between TFAP2A and SCD was performed using ChIP assay and dual-luciferase reporter assay to determine the binding site

cancer and normal bladder mucosa exhibited low methylation levels (beta-value < 0.25, indicating low methylation), with no significant difference between them, suggesting that SCD transcriptional activation is not significantly inhibited by DNA methylation (Fig. 1A) [18].

Next, we performed RT-PCR and WB experiments to detect the mRNA and protein expression of SCD in 10 bladder cancer tissue specimens and common bladder cancer cell lines (RT4, 5637, T24, UMUC3). Correlation statistical analysis of mRNA and protein levels revealed a positive correlation, with $p < 0.05$ and R2 = 0.3496 (Fig. 1B). Subsequently, we conducted a joint analysis of H3K27ac-enriched regions in bladder cancer cell lines (T24, 5637, J82, RT112) using Cistrome and WashU websites (ChIP-seq database), along with observing the conservation of the SCD promoter region in the UCSC database. The results indicated that the core promoter region of SCD in bladder cancer cell lines was located at chr10:100346278–100,348,546 (Fig. 1C, D).

Based on these findings, we constructed a luciferase reporter gene plasmid, pGL3-P (-955 ~ +1314), containing the SCD promoter region. After transfection into RT4 and T24 bladder cancer cell lines, fluorescence intensity was measured using a luminometer. The results demonstrated strong transcriptional activity in this SCD promoter region, with RT4 cells showing higher fluorescence intensity than T24 cells, consistent with the difference in SCD mRNA levels between RT4 and T24 (Fig. 1E).

We then conducted a transcription factor binding site analysis for the core SCD promoter region (-955 ~ +1314) using databases such as HOCOMOCOv11, JASPAR, TRANSFAC, Cistrome, Chipbase, PROMO, htftarget, etc. The analysis identified 11 candidate transcription factors (Fig. 1F). Subsequently, we analyzed the expression levels of these 11 factors in cancer/normal tissues using the TCGA database (Fig. 1G) and explored their correlation with SCD expression in tissues and cell lines using the TCGA and CCLE databases (Fig. 1H, I). We concluded that TFAP2A might be a potential key transcription factor.

Further examination using the HPA database revealed significant staining of TFAP2A protein in bladder cancer (Fig. 1J). TCGA database analysis of TFAP2A expression and its impact on the survival of bladder cancer patients indicated that patients with high TFAP2A expression had poorer survival outcomes (Fig. 1K). Subsequently, using RNAi technology to knock down TFAP2A in UMUC3 cells, we observed a significant downregulation of both SCD mRNA and protein expression (Fig. 1L, M).

To identify the exact binding sites of TFAP2A on the SCD promoter region, we designed a total of 16 PCR primers and performed a ChIP assay using the UMUC3 cell line. The ChIP results revealed that among the 16 possible binding regions, the region targeted by primer 13 was the optimal TFAP2A-DNA binding site. Inference using Jaspar (https://jaspar.genereg.net/) indicated that the 5'-GCCTCCACG-3' (1739 ~ 1747) site in the primer 13 region is a common sequence for TFAP2A to bind DNA (Fig. 1N). To further validate these experimental results, we constructed SCD-p13-promoter-wildtype and SCD-p13-promoter-mutated plasmids (Fig. 1O) and tested whether the mutation at this site affects the binding of TFAP2A to DNA in 293T cells using a dual-luciferase reporter assay. The results showed a significant decrease in the binding ability of TFAP2A to DNA after mutation at this site. In summary, our findings suggest that TFAP2A directly regulates the transcription of SCD in bladder cancer.

SCD inhibitors induce significant apoptosis in bladder cancer stem cells

In our previous studies, we observed that SCD inhibition did not induce notable apoptosis in bladder cancer cell lines that had not been induced into cancer stem cells. However, in cancer stem cells induced from these bladder cancer cell lines, the addition of SCD inhibitors led to a significant induction of apoptosis. As depicted in the figures, treatment with SCD inhibitor A939572 (0.1μM) on adherent cultured bladder cancer cell line UMUC3 and low-adhesion spheroid-induced UMUC3-cancer stem cell (UMUC3-CSC) revealed pronounced apoptosis in UMUC3-CSC, while the same dosage of inhibitor on UMUC3 cells did not induce any apoptosis (Fig. 2A, Figure S1 A and B).

Subsequently, we treated UMUC3 and UMUC3-CSC cells with A939572 (0.1μM) and extracted mRNA to detect changes in apoptosis-related factors such as GRP78, CHOP, and sXBP1 using qRT-PCR. The results

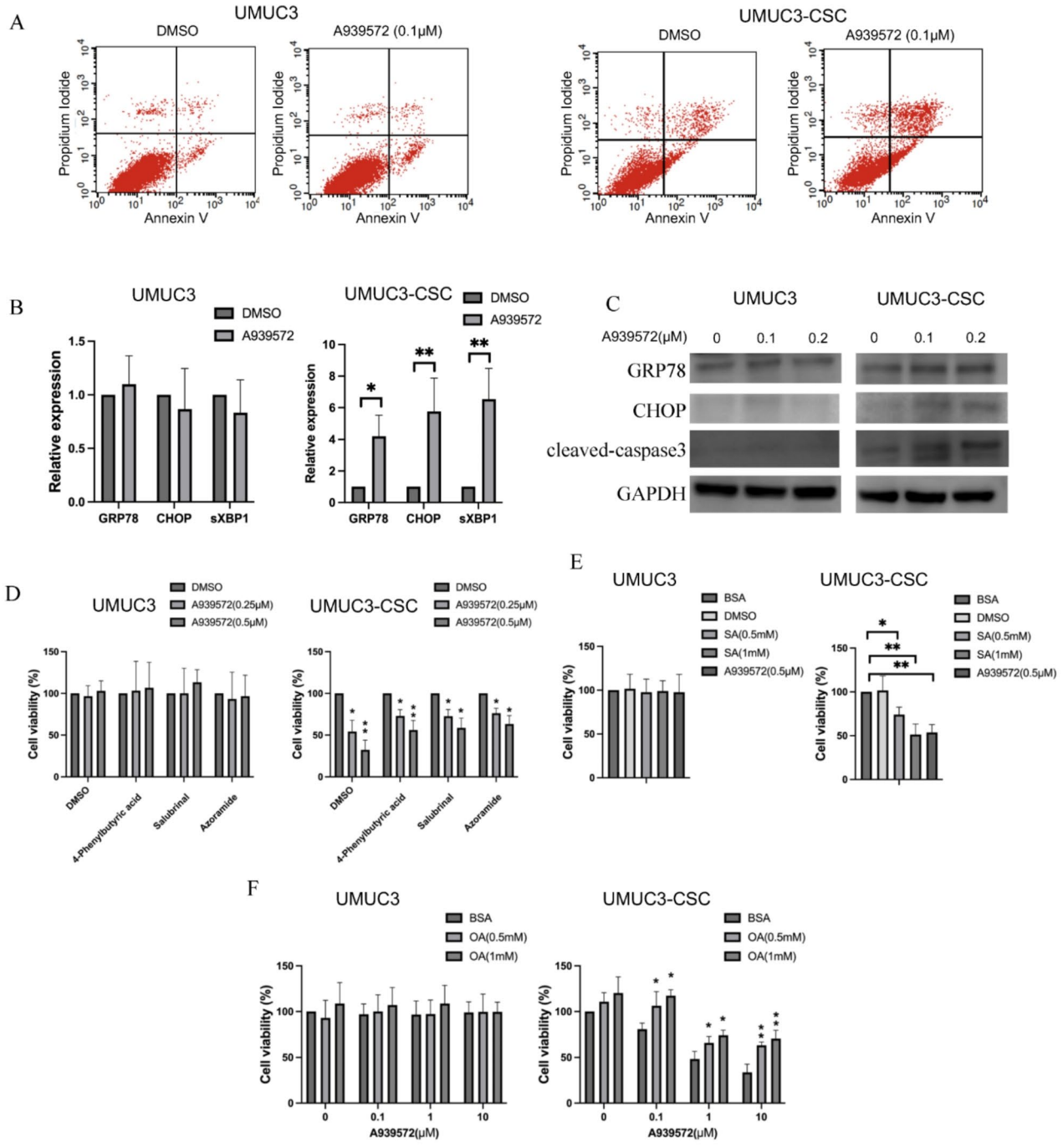

Fig. 2 Inhibitors of SCD trigger substantial apoptosis in CSCs found in bladder cancer. (**A**) SCD inhibitors induced apoptosis in bladder cancer stem cells, sparing non-stem cells (the dosage of SCD inhibitor A939572 is 0.1μM); (**B**) and (**C**) UMUC3-CSC showed notable upregulation of apoptosis-related factors post A939572 treatment; (**D**) In UMUC3-CSC cells, ER stress inhibitors partially restored SCD inhibitor-induced apoptosis; (**E**) Exogenous stearic acid replicated SCD inhibition effects in both groups; (**F**) Treating cells with varied A939572 doses showed OA partly reversed apoptosis. (*: $p < 0.05$, **: $p < 0.01$, ***: $p < 0.005$)

indicated a significant upregulation of the three factors in samples extracted after UMUC3-CSC treatment, whereas no such results were observed in UMUC3 cells (Fig. 2B). Similar protein expression changes of three apoptosis-related factors including GRP78, CHOP, cleaved caspase3 were observed in samples extracted after treatment with similar doses of A939572 (0.1μM and 0.2μM), corresponding to the earlier mRNA level changes (Fig. 2C).

Reports suggest that inhibiting SCD increases the accumulation of intracellular saturated fatty acids, triggering endoplasmic reticulum stress/unfolded protein response-mediated cell death [19]. To investigate this, we used endoplasmic reticulum stress/unfolded protein response-related inhibitors (4-PBA, azoramide, salubrinal) on UMUC3 and UMUC3-CSC cells to observe whether their addition could partially restore the apoptotic effects of A939572 [20–22]. The results showed that in the UMUC3-CSC group, the addition of these three inhibitors indeed partially restored the apoptotic effect induced by SCD inhibition, suggesting that the induction of apoptosis by SCD inhibitors in UMUC3-CSC likely occurs via the endoplasmic reticulum stress/unfolded protein response pathway. As expected, there were no significant changes in the UMUC3 group (Fig. 2D).

In addition to the above evidence, the addition of exogenous saturated fatty acid - stearic acid (SA) in both cell groups showed effects like SCD inhibition (Fig. 2E). Furthermore, treating both cell groups with different concentrations of A939572 (0.1μM, 1μM, 10μM) and simultaneously adding unsaturated fatty acid - oleic acid (OA) to restore the ratio of unsaturated fatty acids/saturated fatty acids, revealed that the exogenous addition of OA partially restored the apoptotic effect induced by SCD inhibition (Fig. 2F).

Considering the comprehensive analysis of the above results, we found that SCD inhibitors notably induce apoptosis in UMUC3-CSC, likely by disrupting the balance between unsaturated and saturated fatty acids, leading to the accumulation of abundant saturated fatty acids, subsequently causing endoplasmic reticulum stress/unfolded protein response, ultimately inducing cell death [23]. In contrast, the UMUC3 cell group did not exhibit a similar phenomenon.

SCD inhibitors significantly enhance sensitivity of bladder cancer stem cells to cisplatin treatment

Cisplatin is commonly used in chemotherapy for bladder cancer treatment. In our previous studies, we found that SCD inhibition did not significantly increase drug sensitivity in bladder cancer cell lines cultured in 2D environments. However, comparative experiments revealed that while treatment with different concentrations of A939572 (0.1μM, 0.25μM, 0.5μM) alongside a fixed concentration of cisplatin did not augment cisplatin's cytotoxic effect in the UMUC3 cell group, SCD inhibition notably enhanced cisplatin-induced cytotoxicity in the UMUC3-CSC group (Fig. 3A).

Studies suggest that SCD inhibition markedly reduces the expression of DNA double-strand repair protein RAD51. We evaluated changes in RAD51 and gamma-H2A.X expression levels in UMUC3 and UMUC3-CSC cells upon A939572 treatment using Western blot. The results showed that while SCD inhibition in UMUC3 cells did not markedly alter the expression of these two proteins, in contrast, in the UMUC3-CSC group, there were notable changes in the expression levels of RAD51 and gamma-H2A.X, indicating a significant decrease in RAD51 expression concurrent with increased SCD inhibition in UMUC3-CSC. This implies that in cancer stem cells, the addition of A939572 partially inhibits DNA damage repair (Fig. 3B).

Subsequently, in the sphere formation assay, the combined treatment of A939572 and cisplatin significantly decreased the number and size of tumor spheres cultured in suspension (Fig. 3C). Building on these findings, we selected RAD51 agonist RS-1 and inhibitor RI-1 (RAD51 inhibitor 1) for validation in synergy and recovery experiments [24, 25]. As depicted in Fig. 3D, in the UMUC3 cell group, under the same concentration of cisplatin, increasing RI-1 concentrations (5μM, 10μM) did not notably increase cell death. Conversely, in the UMUC3-CSC group, RI-1 alone, akin to previous A939572 treatment, induced cell death effectively. Furthermore, under fixed cisplatin concentrations, the addition of RI-1 significantly promoted cell death, indicating that RI-1's inhibition of RAD51 has a similar cytotoxic effect on cancer stem cells as A939572 (Fig. 3D).

Next, within the same grouped cells, we added gradient concentrations of RAD51 agonist RS-1, aiming to validate whether RS-1 addition could partially counteract the increased sensitivity of bladder cancer stem cells to cisplatin induced by A939572. The results revealed that RS-1 addition partially counteracted the combined cytotoxic effect, and this phenomenon was dose-dependent, indicating that using RAD51 agonists can obstruct the heightened cisplatin treatment sensitivity caused by SCD inhibitor (Fig. 3E).

In summary, these experimental results suggest that SCD inhibitors notably augment bladder cancer stem cells' sensitivity to cisplatin treatment, primarily by inhibiting the expression of DNA double-strand repair protein RAD51. The absence of this phenomenon in the UMUC3 cell group is due to the lack of significant expression differences in RAD51 protein.

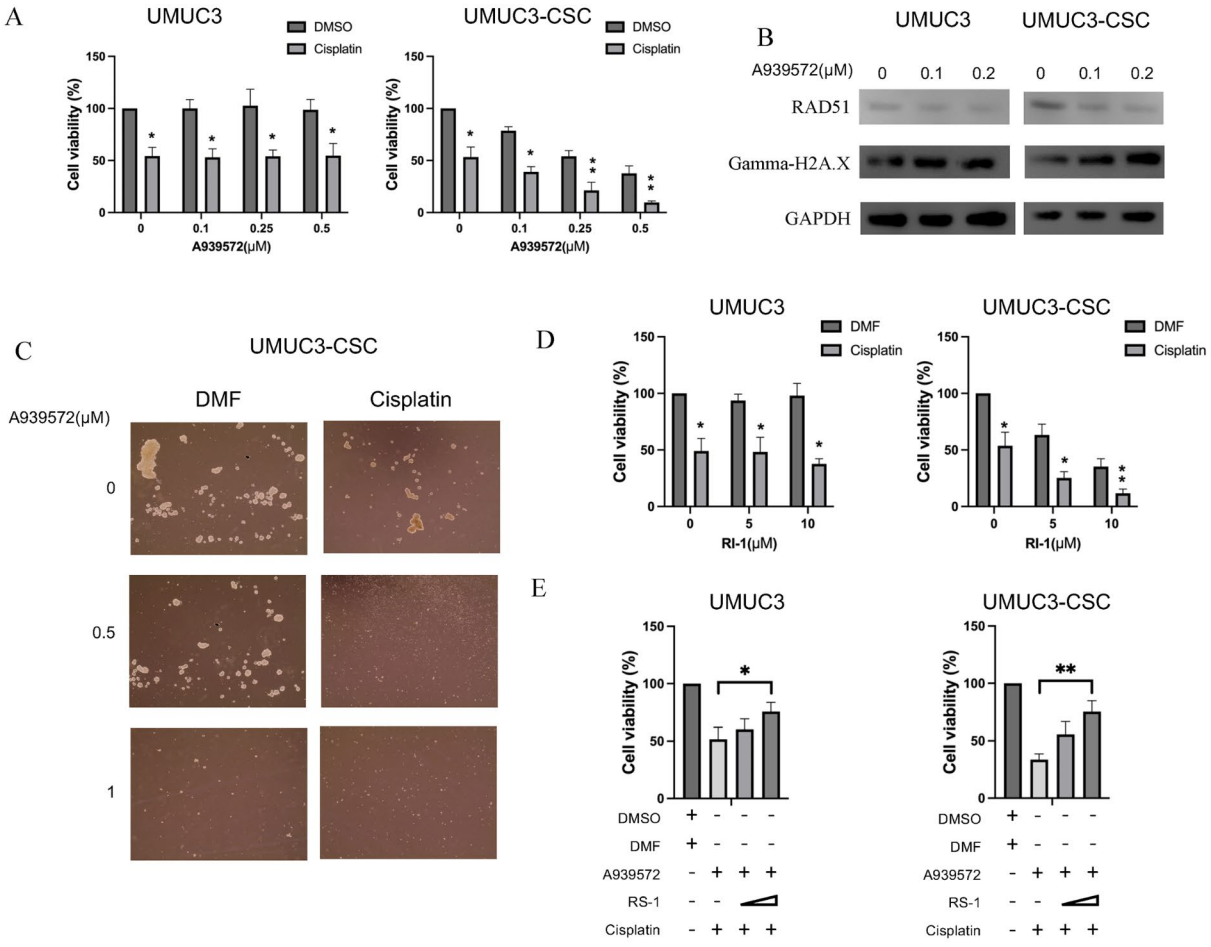

Fig. 3 SCD inhibitors markedly increase cisplatin sensitivity in bladder cancer stem cells. (**A**) Treatment with A939572 and cisplatin didn't boost UMUC3 cytotoxicity, but enhanced UMUC3-CSCs cytotoxicity; (**B**) SCD inhibition reduces RAD51, affecting significantly DNA repair in UMUC3-CSC; (**C**) The joint use of A939572 and cisplatin reduced tumor sphere count and size; (**D**) RAD51 inhibitor RI-1 induces notable cell death in UMUC3-CSC, by enhancing cisplatin effect; (**E**) RS-1 partially reversed A939572's enhanced cisplatin sensitivity in cancer stem cells. (*: $p < 0.05$, **: $p < 0.01$, ***: $p < 0.005$)

SCD inhibition in adherent cultured bladder cancer cells leads to cell cycle arrest rather than apoptosis

In contrast to UMUC3-CSC, adherent-cultured UMUC3 exhibited inconsistent responses to the SCD inhibitor A939572 [17]. This divergence might stem from altered cellular biological functions and lipid metabolic characteristics induced by the conventional suppression of SCD. To observe the impact of SCD inhibition on adherent-cultured UMUC3, we conducted transcriptome sequencing, functional enrichment analysis, and lipid metabolism sequencing. UMUC3 cells were treated with A939572 for 24 h, while the control group received synchronous treatment with 0.1% DMSO. Each set of samples for transcriptome sequencing comprised 3 biological replicates, and for lipid metabolism sequencing, 4 biological replicates were prepared.

The PCA analysis of transcriptome sequencing is depicted in Fig. 4A. In the GO analysis, significant gene expression changes were observed in biological processes like cellular process, metabolic process, and single-organism process, and in molecular functions related to binding and catalytic activity (Fig. 4B). Pathway analysis of differentially expressed genes revealed significant alterations in cell cycle, DNA replication, cytokine-cytokine receptor interaction pathways post A939572 treatment (Figure S2), along with a considerable number of changes in genes highly associated with bladder cancer pathways (Fig. 4C and D). The pathway analysis in the transcriptome sequencing employed the KEGG database annotation, as shown in Fig. 4E. Notably, in the most significantly altered pathway, cell cycle, numerous cell cycle-related factors like CDK2, CDK1, MCM, E2F1, PLK1, PCNA, and CycA were inhibited.

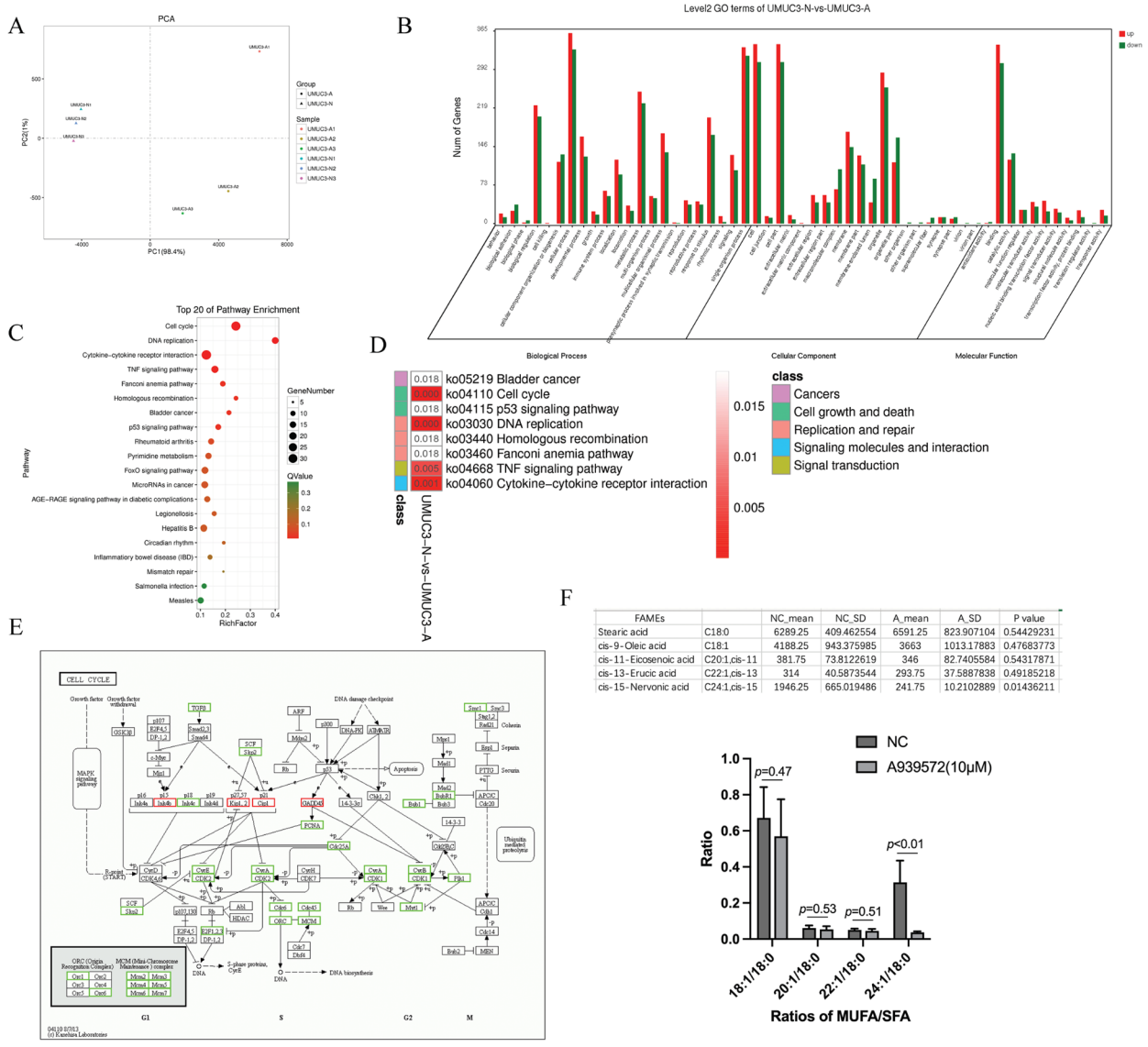

FAMEs		NC_mean	NC_SD	A_mean	A_SD	P value
Stearic acid	C18:0	6289.25	409.462554	6591.25	823.907104	0.54429231
cis-9-Oleic acid	C18:1	4188.25	943.375985	3663	1013.17883	0.47683773
cis-11-Eicosenoic acid	C20:1,cis-11	381.75	73.8122619	346	82.7405584	0.54317871
cis-13-Erucic acid	C22:1,cis-13	314	40.5873544	293.75	37.5887838	0.49185218
cis-15-Nervonic acid	C24:1,cis-15	1946.25	665.019486	241.75	10.2102889	0.01436211

Fig. 4 In adherent bladder cancer cells, SCD inhibition prompts cell cycle arrest over apoptosis. (**A**) The PCA analysis of transcriptome sequencing; (**B**) GO analysis revealed altered gene expression in cellular and metabolic processes, binding, and catalysis; (**C**) and (**D**) A939572 treatment induced changes in cell cycle, DNA replication, and cytokine pathways; (**E**) KEGG analysis indicated cell cycle suppression with downregulation of key factors; (**F**) Lipid sequencing revealed varied oleic and stearic acid levels; Nervonic acid notably changed

The results from lipid metabolism sequencing (Fig. 4F) indicated higher average levels of stearic acid and oleic acid among the detected key lipid metabolites. While the absolute content of oleic acid decreased in cells treated with A939572, there was no significant difference observed in the 18:1/18:0 ratio based on stearic acid content ($p=0.47$). Among other lipid content variations, only Nervonic acid showed a significant difference, markedly downregulated by A939572 (It's important to note that the conversion of saturated to unsaturated fatty acids typically occurs through a chain reaction. As substrates for enzymes involved in fatty acid metabolism, the ratio of product content is often used to indicate the impact of enzyme inhibition on product levels). This suggests that, contrary to the commonly perceived direct substrate effect of SCD on stearic acid/oleic acid, in adherent bladder cancer cell lines, alterations in Nervonic acid content might more sensitively and accurately reflect the effect of SCD inhibition. Overall, these findings suggest that SCD inhibition's impact on adherent-cultured bladder cancer cells predominantly manifests in cell cycle arrest, DNA replication, and functions highly correlated with cell proliferation. This phenomenon may arise due

to the decrease in nervonic acid content rather than the perceived increase in stearic acid/oleic acid ratio.

Supplementing nervonic acid significantly reverses the altered proliferative capacity of adherent-cultured bladder cancer cells induced by SCD inhibition

Based on our preceding experimental findings, we recognized that nervonic acid might be the factor influencing the proliferative capacity of UMUC3 cells. Therefore, we initially conducted real-time cell proliferation assays and observed that the A939572 treatment significantly reduced the proliferative ability of UMUC3 cells, whereas co-treatment with A939572 and nervonic acid noticeably restored the cell proliferation capacity (Fig. 5A). Furthermore, our EdU assay corroborated these effects, indicating that under A939572 (0.25μM) treatment, the proportion of proliferating cells decreased from approximately 20% to around 7%, yet supplementation with nervonic acid significantly counteracted this inhibitory effect on proliferation (Fig. 5B, Figure S1 C). Clone formation assays revealed analogous outcomes, with nervonic acid supplementation not only significantly increasing the number of cell clones but also effectively counteracting the inhibitory effect of A939572 (Fig. 5C).

Apart from the in vitro evidence, to ascertain the in vivo effects, we established a subcutaneous xenograft model in nude mice. The groups were categorized as solvent control, A939572 (A939), A939572+nervonic acid (NA), and both A939572 and nervonic acid were prepared as suspensions for oral gavage twice daily for 28 days. The results indicate that compared to the vehicle group, the overall tumor size in the A939572 group has begun to decrease, but there is no significant statistical difference at the time of euthanasia. Notably, the A939572+nervonic acid group exhibited a significant increase in tumor weight compared to the sole A939572 group, and during the treatment, one mouse in the A939572+nervonic acid group died (Fig. 5D and E). In the A939572 group, two model animals developed soft

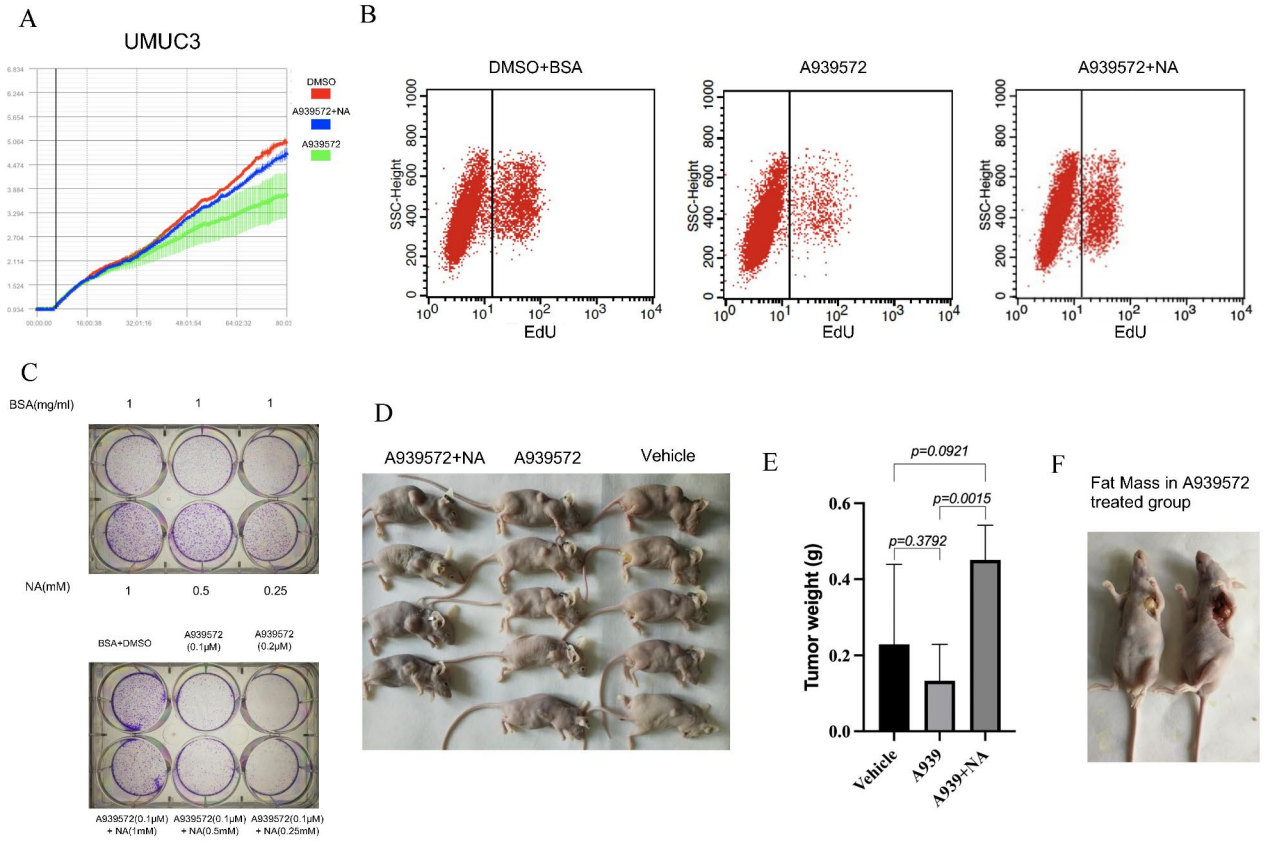

Fig. 5 Adding Nervonic Acid (NA) Reverses SCD Inhibition's Impact on Bladder Cancer Cell Proliferation. (**A**) Nervonic acid restoration counteracts UMUC3 cell proliferation reduction caused by A939572 treatment; (**B**) A939572 treatment reduced cell proliferation and nervonic acid supplementation counteracted this effect; (**C**) Nervonic acid supplementation counters A939572's inhibitory effect, enhancing cell clone formation; (**D**) and (**E**) In the xenograft model, A939572 reduced tumor size; adding nervonic acid increased tumor weight and also increased the risk of death as depicted in the A939572 + NA group; (**F**) In the A939572-treated group, two model animals exhibited soft lumps in the armpit area, confirmed as adipose tissue upon dissection. (In the A939572 + NA treatment group, one mouse died during the mid-course of the experiment and was excluded from the statistical analysis)

lumps in the axillary region, which upon dissection were identified as fat granules (Fig. 5F).

These combined in vivo and in vitro results unequivocally demonstrate that the addition of nervonic acid significantly counteracts the reduced proliferative capacity induced by SCD inhibition in bladder cancer cells. Additionally, our animal experiments unexpectedly revealed that the use of A939572 might lead to abnormal fat granule formation.

Discussion

This study serves as a follow-up investigation to the prior research concerning the biological mechanisms of SCD in bladder cancer. In our earlier study, we comprehensively elucidated the biological functions of SCD in bladder cancer and its impact on bladder cancer patients. Employing serum-free induction methods, we suspended bladder cancer cell lines to induce their transformation into tumor stem cells. These tumor stem cells, subjected to microarray assays, led to the identification of differentially expressed genes (DEGs). Subsequently, through joint analysis involving Oncomine and TCGA databases, we highlighted the crucial role of SCD within bladder cancer stem cells [17]. However, three issues gradually emerged during the study. Firstly, the underlying cause of the abnormally high expression of SCD in bladder cancer. Secondly, we noted a significant decline in the proliferative capacity of bladder cancer cells under the influence of SCD inhibitors in a 2D adherent culture environment; however, cellular survival remained unaffected, and apoptotic phenomena did not occur under SCD inhibition. Interestingly, significant apoptosis was observed in suspended culture cancer stem cells. Lastly, the SCD inhibitors failed to enhance the chemotherapeutic drug sensitivity in adherent bladder cancer cells, yet significantly increased chemotherapeutic drug sensitivity in cancer stem cells under SCD inhibition. Considering these experimental findings, we conducted this present study.

This study can be broadly divided into two parts. The first part aims to address the abnormally high expression of SCD in bladder cancer. In evaluating the methylation levels of the SCD promoter region, subsequent detection across various types of bladder cancer samples (cell lines and tissues) revealed a positive correlation between SCD mRNA/protein levels and confirmed their low methylation levels in the SCD promoter region. Further joint analysis using different databases identified multiple transcription factors, among which TFAP2A played the most significant role. Through ChIP experiments and luciferase reporter gene assays, we further confirmed the direct binding ability of this transcription factor to the SCD promoter region and identified the binding sites.

In the second part, we first clarified the differing responses of cancer stem cells and adherent tumor cells to drugs. Through literature review and experiments, we demonstrated that SCD inhibitors could increase the accumulation of intracellular saturated fatty acids, thereby inducing endoplasmic reticulum stress/unfolded protein response and leading to cell death. This effect could be reversed by the addition of monounsaturated fatty acids. Compared to cancer stem cells, adherent cells exhibited significantly weaker responses and did not manifest notable apoptotic effects under effective SCD concentrations. Additionally, through RNA-seq combined with fatty acid metabolism profiling, we found that SCD inhibition in adherent cells primarily led to pathway alterations associated with cell proliferation/cell cycle/DNA replication. This effect aligned with our prior experimental results and suggested that, compared to the conventional assumption of an increase in OA/SFA ratio [26], the more likely cause was the significant decrease in nervonic acid levels, which might be more sensitive to SCD activity changes.

Currently, most research on SCD in tumors primarily focuses on the impact of lipid metabolism on tumors [27]. Studies related to drug sensitivity are limited, and from the current data, most reports suggest that SCD inhibition can enhance tumor drug sensitivity [28]. However, studies investigating the differential responses of different types of tumor cells to drugs are relatively scarce. Cancer cells exhibit heterogeneity, and one of the reasons behind this heterogeneity may be associated with cancer stem cells (CSCs). The experimental evidence for CSCs was first described in hematology [29, 30]. According to the consensus definition of CSCs [31], these cells possess the ability for self-renewal and can generate various types of cancer cells that comprise the tumor. Cells possessing CSC-like characteristics generally exhibit increased resistance to drugs [32]. However, our study found that selecting appropriate targets might distinguish tumor cells with CSC-like features, making them more susceptible to drug-induced damage.

Nevertheless, our research has several limitations. Firstly, although we identified the crucial transcription factor TFAP2A associated with SCD overexpression in bladder cancer, transcriptional regulatory mechanisms for a single factor are often complex and variable [33]. Due to limitations, we could not formulate a clear transcriptional regulatory network and couldn't fully distinguish the transcription factors and auxiliary factors involved in SCD overexpression. Secondly, although we experimentally demonstrated that inhibiting SCD led to increased apoptosis in CSCs, and this effect could be attributed to endoplasmic reticulum stress/unfolded protein response, adherent cells did not exhibit this phenomenon under the influence of SCD inhibitors. We speculate

that this phenomenon might be due to a mechanism present in adherent cells that counteracts endoplasmic reticulum stress/unfolded protein response, but the specific reasons need further exploration. Finally, there are limited reports on the relevance of nervonic acid in tumor diseases, primarily concentrated in nutrition and metabolism fields [34, 35]. The significant decrease in nervonic acid due to SCD inhibition in bladder cancer is the first reported observation in our previous studies. It is particularly noteworthy that in animal experiments, while the average tumor mass in the group treated with A939572 alone showed a reduction compared to the control group, this difference did not reach statistical significance. This observation suggests that our treatment regimen may require refinement, such as employing a more potent SCD inhibitor or prolonging the duration of drug administration. Regrettably, the experiment was prematurely terminated due to observed mortality in the group receiving additional nervonic acid, preventing further extension of the treatment period. Therefore, further in-depth research is required to elucidate the relevant functions of nervonic acid in bladder cancer and other cancer types.

In conclusion, our study indicates that the high expression of SCD in bladder cancer might be highly correlated with the activation of TFAP2A at its transcriptional level. Within CSCs, the effects demonstrated by SCD inhibitors might possibly be attributed to endoplasmic reticulum stress.

Supplementary Information

The online version contains supplementary material available at https://doi.org/10.1186/s12935-024-03540-w.

Supplementary Material 1

Author contributions

Yuchen Li: Conceptualization, Formal Analysis, Methodology, Validation, Visualization, Writing–original draft. Chiyuan Piao: Conceptualization, Data curation, Methodology, Investigation, Project administration, Writing–review and editing. Chuize Kong: Conceptualization, Funding acquisition, Project administration, Resources, Supervision, Writing–review and editing.

Funding

This work was supported by the 69th China Postdoctoral Science Foundation (2021M693916), Shenyang Clinical Medical Research Center (Grant No. 20-204-4-42), Liaoning Clinical Medical Research Center (Grant No. [2020] 44) and Natural Science Foundation of Liaoning Province (2019-MS-378), Precision Medicine Research on Urological Diseases (Project ID: 2023JH6/100200010). The authors declare no competing financial interests. Funding agency did not participate in the design of the study or collection, analysis and interpretation of data or writing the manuscript.

Data availability

The raw data supporting the conclusion of this article will be made available by the authors, without undue reservation. The raw data of RNA-seq mentioned in the article can be accessed via the following link: https://www.ncbi.nlm.nih.gov/bioproject/PRJNA1048080.

Declarations

Ethics approval

The Animal Ethics and Welfare Committee of China Medical University had provided approval before all the animal experiments performed.

Competing interests

The authors declare no competing interests.

Received: 29 July 2024 / Accepted: 17 October 2024
Published online: 29 October 2024

References

1. Siegel RL, Miller KD, Wagle NS, Jemal A. Cancer statistics, 2023. CA Cancer J Clin. 2023;73(1):17–48.
2. Siegel RL, Miller KD, Jemal A. Cancer statistics, 2020. CA Cancer J Clin. 2020;70(1):7–30.
3. Chen W, Zheng R, Baade PD, Zhang S, Zeng H, Bray F, et al. Cancer statistics in China, 2015. CA Cancer J Clin. 2016;66(2):115–32.
4. Kamoun A, de Reynies A, Allory Y, Sjodahl G, Robertson AG, Seiler R, et al. A consensus molecular classification of muscle-invasive bladder cancer. Eur Urol. 2020;77(4):420–33.
5. Yatai KB, Dunning MJ, Wang D. Consensus genomic subtypes of muscle-invasive bladder cancer: a step in the right direction but still a long way to go. Eur Urol. 2020;77(4):434–5.
6. Shkolyar E, Jia X, Chang TC, Trivedi D, Mach KE, Meng MQ, et al. Augmented bladder tumor detection using deep learning. Eur Urol. 2019;76(6):714–8.
7. Moschini M, Shariat SF, Black P, Kamat AM, Stabile A, Cathelineau X, et al. Do not learn a technique, learn the biology underlying the disease: techniques evolve, biology prevails. Eur Urol. 2020;77(1):1–2.
8. Gore JL, Wright JL. Can we prevent bladder cancer recurrences? Eur Urol. 2019;75(4):602–3.
9. AM AL, Syed DN, Ntambi JM. Insights into Stearoyl-CoA Desaturase-1 regulation of systemic metabolism. Trends Endocrinol Metab. 2017;28(12):831–42.
10. Kubota CS, Espenshade PJ. Targeting Stearoyl-CoA desaturase in solid tumors. Cancer Res. 2022;82(9):1682–8.
11. Kikuchi K, Tsukamoto H. Stearoyl-CoA desaturase and tumorigenesis. Chem Biol Interact. 2020;316:108917.
12. Tracz-Gaszewska Z, Dobrzyn P. Stearoyl-CoA desaturase 1 as a therapeutic target for the treatment of Cancer. Cancers (Basel). 2019;11(7).
13. Takada R, Satomi Y, Kurata T, Ueno N, Norioka S, Kondoh H, et al. Monounsaturated fatty acid modification of wnt protein: its role in wnt secretion. Dev Cell. 2006;11(6):791–801.
14. Rios-Esteves J, Resh MD. Stearoyl CoA desaturase is required to produce active, lipid-modified wnt proteins. Cell Rep. 2013;4(6):1072–81.
15. Kim H, Rodriguez-Navas C, Kollipara RK, Kapur P, Pedrosa I, Brugarolas J, et al. Unsaturated fatty acids stimulate tumor growth through stabilization of beta-catenin. Cell Rep. 2015;13(3):495–503.
16. Min JY, Kim DH. Stearoyl-CoA desaturase 1 as a therapeutic biomarker: focusing on cancer stem cells. Int J Mol Sci. 2023;24(10).
17. Piao C, Cui X, Zhan B, Li J, Li Z, Li Z, et al. Inhibition of stearoyl CoA desaturase-1 activity suppresses tumour progression and improves prognosis in human bladder cancer. J Cell Mol Med. 2019;23(3):2064–76.
18. Kulis M, Esteller M. DNA methylation and cancer. Adv Genet. 2010;70:27–56.
19. Eyme KM, Sammarco A, Jha R, Mnatsakanyan H, Pechdimaljian C, Carvalho L, et al. Targeting de novo lipid synthesis induces lipotoxicity and impairs DNA damage repair in glioblastoma mouse models. Sci Transl Med. 2023;15(679):eabq6288.
20. Shu S, Wang H, Zhu J, Fu Y, Cai J, Chen A, et al. Endoplasmic reticulum stress contributes to cisplatin-induced chronic kidney disease via the PERK-PKCdelta pathway. Cell Mol Life Sci. 2022;79(8):452.
21. Fu S, Yalcin A, Lee GY, Li P, Fan J, Arruda AP, et al. Phenotypic assays identify azoramide as a small-molecule modulator of the unfolded protein response with antidiabetic activity. Sci Transl Med. 2015;7(292):292ra98.
22. Uzay B, Houcek A, Ma ZZ, Konradi C, Monteggia LM, Kavalali ET. Neurotransmitter release progressively desynchronizes in induced human neurons during synapse maturation and aging. Cell Rep. 2023;42(2):112042.
23. Thurmer M, Gollowitzer A, Pein H, Neukirch K, Gelmez E, Waltl L, et al. PI(18:1/18:1) is a SCD1-derived lipokine that limits stress signaling. Nat Commun. 2022;13(1):2982.

24. Arnoult N, Correia A, Ma J, Merlo A, Garcia-Gomez S, Maric M, et al. Regulation of DNA repair pathway choice in S and G2 phases by the NHEJ inhibitor CYREN. Nature. 2017;549(7673):548–52.
25. Hu X, Hao F, Li X, Xun Z, Gao Y, Ren B, et al. Generation of VEGF knock-in Cashmere goat via the CRISPR/Cas9 system. Int J Biol Sci. 2021;17(4):1026–40.
26. Chan KS, Cheung SM, Senn N, Husain E, Masannat Y, Heys S, et al. Peritumoural spatial distribution of lipid composition and tubule formation in breast cancer. BMC Cancer. 2022;22(1):285.
27. Piccinin E, Cariello M, Moschetta A. Lipid metabolism in colon cancer: role of liver X receptor (LXR) and Stearoyl-CoA desaturase 1 (SCD1). Mol Aspects Med. 2021;78:100933.
28. Wong TL, Loh JJ, Lu S, Yan HHN, Siu HC, Xi R, et al. ADAR1-mediated RNA editing of SCD1 drives drug resistance and self-renewal in gastric cancer. Nat Commun. 2023;14(1):2861.
29. Fialkow PJ, Jacobson RJ, Papayannopoulou T. Chronic myelocytic leukemia: clonal origin in a stem cell common to the granulocyte, erythrocyte, platelet and monocyte/macrophage. Am J Med. 1977;63(1):125–30.
30. Bonnet D, Dick JE. Human acute myeloid leukemia is organized as a hierarchy that originates from a primitive hematopoietic cell. Nat Med. 1997;3(7):730–7.
31. Clarke MF, Dick JE, Dirks PB, Eaves CJ, Jamieson CH, Jones DL, et al. Cancer stem cells–perspectives on current status and future directions: AACR workshop on cancer stem cells. Cancer Res. 2006;66(19):9339–44.
32. Lytle NK, Ferguson LP, Rajbhandari N, Gilroy K, Fox RG, Deshpande A, et al. A multiscale map of the stem cell state in pancreatic adenocarcinoma. Cell. 2019;177(3):572–86 e22.
33. Lambert SA, Jolma A, Campitelli LF, Das PK, Yin Y, Albu M, et al. The human transcription factors. Cell. 2018;172(4):650–65.
34. Li Q, Chen J, Yu X, Gao JM. A mini review of nervonic acid: source, production, and biological functions. Food Chem. 2019;301:125286.
35. Phung NV, Rong F, Xia WY, Fan Y, Li XY, Wang SA et al. Nervonic acid and its sphingolipids: biological functions and potential food applications. Crit Rev Food Sci Nutr. 2024;64(24):8766-8785.

Publisher's note